Aortic Flow Hemodynamics after Surgical Aortic Valve Replacement: Comparison with a Healthy Subject

Selene Pirola[1,*], Zhuo Cheng[1], Omar A. Jarral[2], Declan P. O'Regan[3], Thanos Athanasiou[2], Xiao Y. Xu[1].

1 Department of Chemical Engineering, Imperial College London, UK
2 Department of Surgery and Cancer, St. Mary's Hospital, Imperial College London, UK
3 Institute of Clinical Science, Hammersmith Hospital, Imperial College London, UK

* Correspondence: s.pirola@imperial.ac.uk, Department of Chemical Engineering, Imperial College London, South Kensington Campus, SW7 2AZ, London, UK.

1. Introduction

Aortic stenosis (AS) is a life-threatening disease involving a narrowing of the aortic valve orifice, which can compromise aortic hemodynamic functions or lead to heart failure. This disease affects millions of people in the world and if left untreated can lead to death soon after the onset of symptoms [1]. Therefore, AS has to be accurately followed-up and corrected through valve replacement, with surgical aortic valve replacement (SAVR) being the treatment of choice for this disease.

Despite being a life-saving procedure, SAVR can alter aortic flow patterns, possibly influencing aortic endothelial function and organ perfusion [2]. It is already well known that a disturbed hemodynamic environment in the aorta can lead to life-threatening diseases, such as aortic aneurysm and dissection, but very few computational studies have investigated the effects of these replacement techniques on aortic fluid dynamics.

Computational fluid dynamics (CFD) can be used to simulate aortic hemodynamics, and the combination of CFD and magnetic resonance imaging (MRI) techniques has become the main method for cardiovascular fluid dynamics evaluation. In this study, the aortic hemodynamics of a healthy patient was compared against a patient who underwent SAVR. Patient-specific geometries employed in CFD models were obtained from MRI scans. A physiological set of boundary conditions (BCs) was applied: patient-specific velocity profiles extracted from phase-contrast MRI (PC-MRI) were prescribed at the model inlet, thus accounting for the strong influence that inlet velocity distribution has on aortic hemodynamics and wall shear stress [3]; 3-element Windkessel (3-EWM) model was applied at all the model outlets.

2. Materials and Methods

MR scans were performed on a patient (PA), who underwent a mechanical aortic valve replacement and graft-conduit implantation, and a sex-matched healthy volunteer (HV) at the Robert Steiner MRI Unit at Hammersmith Hospital (London, UK) using a 1.5T Philips Achieva system (Best, Netherlands). Multi-slice sagittal anatomic images of the thoracic aorta and proximal vessels were acquired using a navigator-gated balanced steady-state free precession angiogram (voxel size 0.5x0.5x2 mm). PC-MRI planes were placed at the level of the annulus and the pulmonary bifurcation, normal to the aortic axis with three-dimensional velocity encoding. Velocity encoding parameters (VENC) were set to be 10% above the peak velocity for each velocity component. In-plane pixel resolution and slice thickness were 1.4 mm x 1.4 mm and 10 mm, respectively, and 100 time points in an average cardiac cycle were obtained using retrospective cardiac gating. For both subjects, pressure measurements were taken 30 min prior to the MR scan by using a BP Plus device (BP Plus, Uscom, Australia). The HV had no medical history of cardiovascular pathologies, and both PA and HV gave their informed consent.

Patient-specific 3D aortic geometries, inclusive of the arch branches, were reconstructed from the acquired MR images by using Mimics (v18.0.0.525, Materialise, Leuven, Belgium). An *in-house* MATLAB (The MathWorks Inc., Natick, MA, United States) tool was used to correct for image noise

and manually segment the PC-MRI images. A structured mesh was generated using ANSYS ICEM (v15.0, ANSYS Inc., Canonsburg, PA). The obtained meshes consisted of approximately 1.5 and 2 million hexahedral elements for HV and PA, respectively.

The model inlet was located at the level of the aortic root, where PC-MRI flow mapping was acquired. 3D time-varying velocity profiles of the entire cardiac cycle were reconstructed from segmented PC-MRI and mapped to the 3D global coordinates of the computational model, thus imposing 3D velocity profiles as inlet boundary conditions (Fig.1). At each of the model outlets (3 in the arch and 1 in the descending aorta), 3-EWM was applied with its coefficients being calculated employing the acquired PC-MRI data and pressure waveform; this was to account for the influence of the vasculature distal to the model outlet [4].

Numerical solutions were obtained using ANSYS CFX (v15.0, ANSYS, Canonsburg, PA, USA). In each case, the simulation continued until a converged cyclic solution was reached. The flow was assumed to be laminar and blood was considered as a Newtonian fluid, with viscosity (μ) of 0.004 Pa·s and a density (ρ) of 1060 kg/m^3. Instantaneous streamlines from CFD results were obtained using ANSYS CFD-Post (v15.0, ANSYS, Canonsburg, PA, USA) and wall shear stress (WSS) maps were obtained with CEI Ensight (v10.1, CEI Inc., Apex, NC, USA).

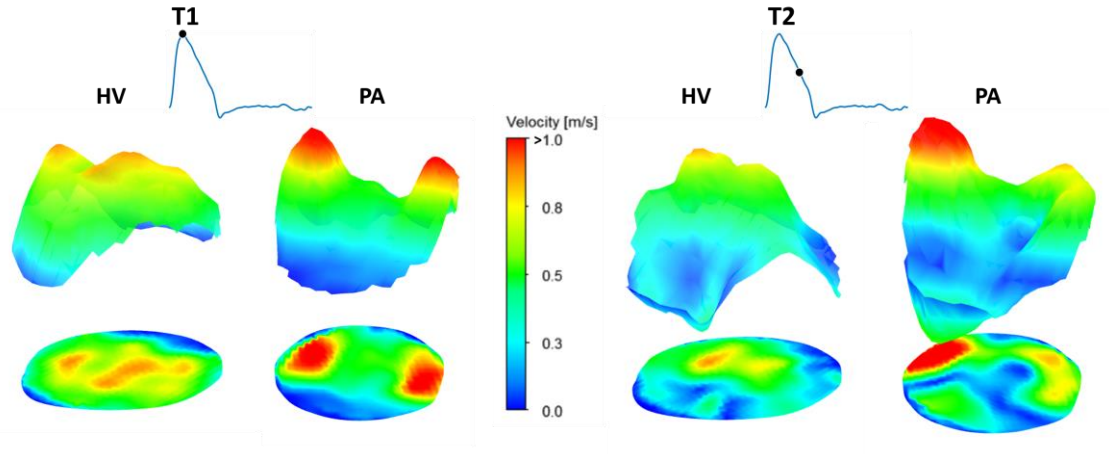

Figure 1: Velocity profiles used as inlet boundary condition. Time points corresponding to peak-systole (T1) and mid-systolic deceleration phase (T2) are shown for both subjects. The same scale (0-1 m/s) was used to allow direct comparison, but values varied between the two subjects: at T1 velocity peaks were 0.87 and 1.1 m/s, at T2 of 0.86 and 1.2 m/s, for HV and PA, respectively.

3. Results

Flow Patterns. Fig.2 shows instantaneous streamlines at peak-systole (T1) and mid-systolic deceleration phase (T2). At peak systole, flow patterns in PA were similar to those found in HV, but small recirculation zones (marked by blue arrows) were observed near the inlet and in the mid-ascending aorta (AAo), where the transition from graft to the patient's aorta caused an abrupt change in the geometry. At T2, PA presented a chaotic flow pattern in the inner-AAo with a flow jet (marked by red arrows) emerging from the outer-right part of the inlet and impinging the aortic wall along the entire AAo and the aortic arch (AA) until the junction of the third branch. Large regions of recirculation can be observed in the patient's AAo and AA (blue arrows), downstream of the suture line between the conduit and aorta. Helical flow was observed in both subjects.

Wall shear stress. Time average wall shear stress (TAWSS) and oscillatory shear index (OSI) were evaluated based on instantaneous WSS values [5]. PA presented higher values of TAWSS (Fig. 3), with a peak value equal to 14.3 Pa, while HV presented a maximum value of 4.3 Pa. A more variable distribution of TAWSS was also noted in PA, with high values along the path followed by the flow jet observed in mid-systole. In both cases, branch junctions presented the highest TAWSS, but PA's absolute values were higher. Regions of low TAWSS were observed in the AAo and AA of PA, where

flow recirculation occured. However a wide region of low TAWSS was also observed in the AA of HV. In both cases, overall lower TAWSS values were observed in the descending aorta (DAo).

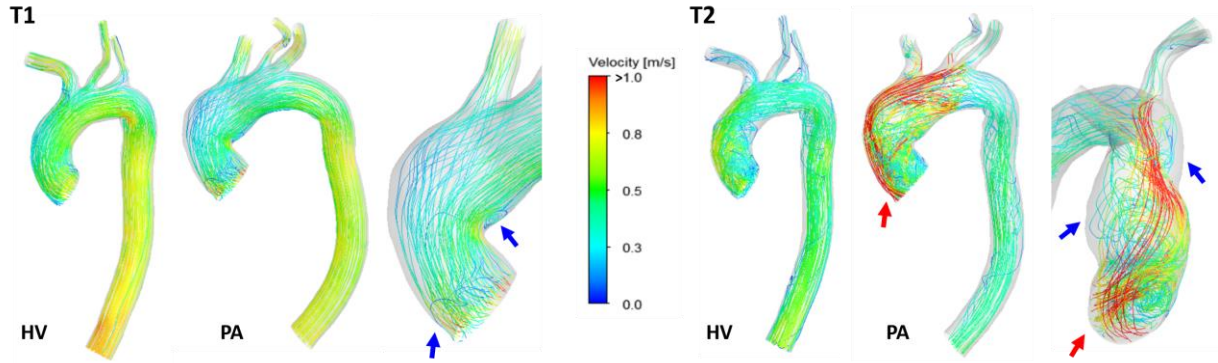

Figure 2: Instantaneous velocity streamlines in the healthy subject (HV) and in the patient (PA) at time-points T1 and T2. For both subjects left-oblique views are shown, for PA details of the AAo are also shown (right figure at both time points). Blue arrows indicate recirculation regions; red arrows highlight the flow jet observed in mid-systole.

The OSI distribution (Fig. 4) presented values up to the upper limit (0.5) in the AA of both subjects. For the HV a wide band of high OSI was present at the root of the brachiocephalic artery, while for PA it was between the junctions of the left common carotid and left subclavian arteries. Smaller regions of high OSI were also noted in the mid-AA of HV, in the AAo of PA, and in the DAo of both subjects. OSI and TAWSS distributions showed that some regions of high OSI overlapped with areas of low TAWSS in both HV and PA. Since low and oscillatory wall shear stress has been suggested as atherogenic, it would be useful to evaluate indices that combine OSI and TAWSS.

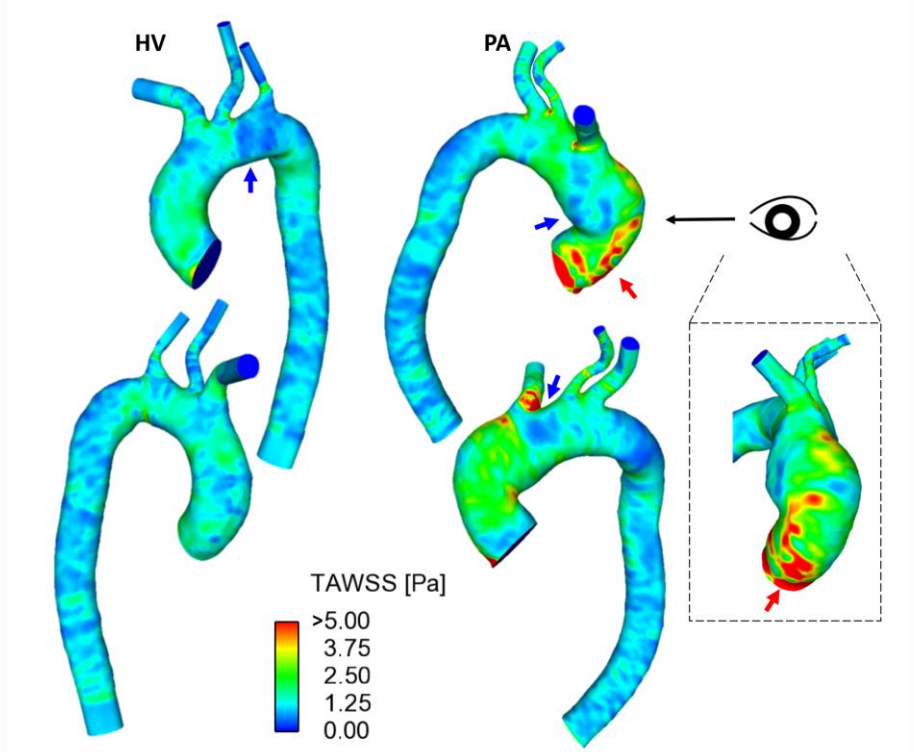

Figure 3: TAWSS contours for HV (left) and PA (right). The same scale (0-5 Pa) was used to allow direct comparison but values varied between the two subjects, with peaks of 4.3 Pa and 14.3 Pa for HV and PA, respectively. Top: right-oblique view, bottom: left-oblique view. For PA a frontal view (right, dashed square) is also shown. Red arrows indicate high TAWSS regions; blue arrows indicate regions with low values of TAWSS.

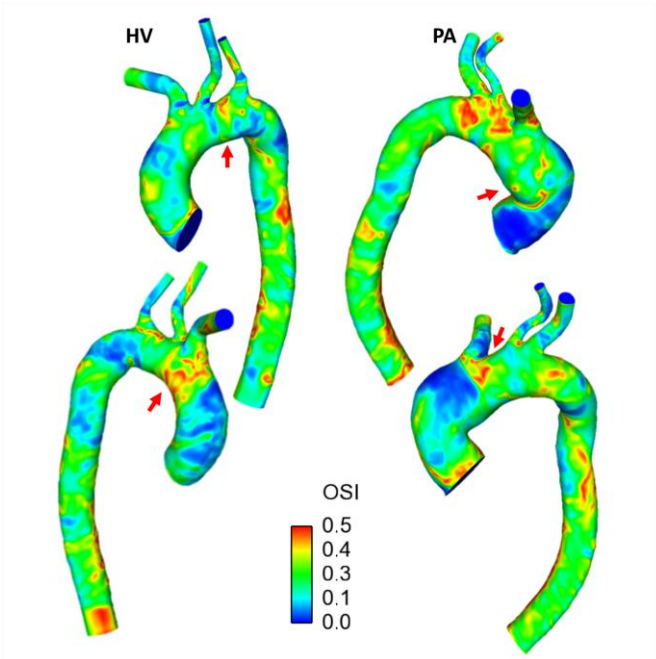

Figure 4: OSI contours for HV (left) and PA (right). Top: right-oblique view, bottom: left-oblique view. Arrows indicate areas with high OSI.

4. Discussion and Conclusions

Overall, the PA's aorta presented velocity values higher than that of HV. The analysis of flow patterns showed that normal flow was restored by SAVR at peak systole. At this time point the velocity patterns of PA closely resembled that of HV, without presenting the high velocity jet commonly found in patients with AS [5]. Recirculation zones were observed at T1 in both subjects. At mid-systolic deceleration (T2), flow in the PA's aorta was more chaotic when compared to that of HV. In particular, the altered pattern observed in the AAo might be related to the mechanical valve, while the recirculation regions observed in the AA may be caused by the abrupt change in the geometry. The flow jet observed in the AAo of PA is probably due to the mechanical valve closure, and seems to be responsible for the higher TAWSS values in PA than HV. The peak TAWSS for PA was about 3-times the maximum value for HV: high wall shear stress may cause aortic matrix degeneration, potentially leading to aortic wall enlargement or aneurysm. Low and oscillatory WSS was observed in the PA's AA, where recirculation regions were found. These regions were further analysed in terms of endothelial cell activation potential (ECAP) and other hemodynamic wall indices, and detailed discussion of these results will be presented in a full paper.

The approach employed in this work, combining computational modelling with realistic boundary conditions derived from PC-MRI data, allowed for a patient-specific evaluation of the hemodynamics performance of SAVR. Future studies will include more cases in order to assess the hemodynamic performance of different aortic replacement procedures.

Acknowledgement

This work was supported by the European Commission within the Horizon 2020 Framework through the MSCA-ITN European Training Networks (project number 642458) and the National Institute for Health Research Biomedical Research Centre based at Imperial College Healthcare NHS Trust and Imperial College London.

5. References

1. Ross J. et al., Circulation 1968; 38(1):61-67
2. Cheng Z. et al., Ann.Biomed. Eng. 2016; 44(5): 1392-1404
3. Mahadevia R. et al., Circulation 2014; 129(6): 673-682
4. Xiao N. et al., Int. J. Numer. Method Biomed. Eng. 2014; 30(2): 204-231
5. Tan F. et al., Cardiovasc. Eng. Technol. 2012; 3(1): 123-135